Advances in Differential Equations and Control Processes 2025, 32(3), 3444.
doi: https://doi.org/10.59400/adecp3444

Article

Partial differential analytical expression for the failure rate change of electrical components under multi-fault coupling

Tiejun Cui[1,2], Pengpeng Wei[1], Shasha Li[1,2,*]

[1] School of Environmental and Chemical Engineering, Shenyang Ligong University, Shenyang 110159, China
[2] Liaoning Safety Engineering Industry School, Shenyang Ligong University, Shenyang 110159, China
*** Corresponding author:** Shasha Li, lsslntu@163.com

CITATION

Cui T, Wei P, Li S. Partial differential analytical expression for the failure rate change of electrical components under multi-fault coupling. Advances in Differential Equations and Control Processes. 2025; 32(3): 3444. https://doi.org/10.59400/adecp3444

ARTICLE INFO

Received: 25 June 2025
Revised: 23 August 2025
Accepted: 27 September 2025
Available online: 30 September 2025

Abstract: With the trend of high integration and complex working conditions of electronic equipment, multi-fault coupling failures have become a key threat to operational reliability. To study the influence mechanism of multi-factor-induced multi-fault modes on the failure of electrical components and consider the time-dependent effect of component operation, an analytical expression in the form of a partial differential equation for the component failure rate is established. The time-dependent of failure rate, multi-fault coupling terms, and coupling coefficients in the expression are further determined. The research shows that constructing the partial differential expression for failure rate should consider electromigration, corrosion, hot carrier, and dielectric breakdown faults and their influencing factors. By introducing multi-fault coupling terms, the impacts of parameters such as temperature, current density, etc. on various fault modes and component failure rates are reflected. Electromigration-corrosion, heat-carrier-dielectric breakdown accelerate the occurrence of faults, and the analytical and approximate formulas for coupling coefficients are provided. Case analysis obtains the failure rates of each fault, the component failure rate, and two coupling coefficients; and it is found that the failure rate changes significantly at 100 s, serving as a critical life point. This study provides a method for analyzing the failure rate of electrical components under multi-factor influences over time.

Keywords: safety system engineering; electrical components; multi-fault coupling; factor influence; failure rate; partial differential

1. Introduction

The failure of electrical components under multi-fault coupling is common in industries such as electronics and electric power. From consumer electronics to industrial equipment, electrical components are often affected by multiple fault synergistic influences such as electromigration and corrosion. At present, although there are basic models for these problems, the calculation and analysis of multi-fault coupling still face difficulties, and it is even more difficult to adapt to complex working conditions. The failure of electrical components under multi-fault coupling has important research significance. Non-linear parameter fitting and model prediction of complex working conditions are practical and difficult problems. However, studying the failure mechanism is of great significance for reasonably designing component failure rate prediction accuracy, optimizing design and operation and maintenance, ensuring the reliable operation of equipment, and avoiding major accidents. With the development of electronic equipment towards high integration and complex working conditions, the

hidden danger of failures is also increasing. Therefore, researching the multi-fault coupling effect on the failure rate of electrical components is urgent, which is related to the safety production of electrical and electronic-related industries.

There is a lot of research on the failure of electrical and electronic components under complex environments of multi-faults and multi-factors. The research focuses on multiple key issues in the electrical power system. In terms of fault detection and prediction, Dwivedi D et al. [1] uses nonlinear dynamics and machine learning models to achieve fault detection and prediction in distribution systems, while Ilyushin P et al. [2] proposes an algorithm to identify the possibility and development trajectory of cascading failures in power systems. For fault diagnosis of energy storage systems, Lou Y-L et al. [3] focuses on the detection of damaged units in lithium battery thermal management systems, and Shuhui W et al. [4] uses convolutional neural networks to infer the fault causes of onboard lithium-ion battery thermal runaway. In the study of fault mechanisms in new energy devices, Qi M et al. [5] analyzes the electrical failure and stability of perovskite solar cells under reverse bias. At the level of electrical components and connection systems, Ren L et al. [6] investigates the mechanism and dynamic characteristics of intermittent failures in electrical connectors, and An H et al. [7] applies rough number projection to conduct multi-perspective failure mode and effects analysis. Regarding the reliability of coupled systems, Lu Q-C et al. [8] models the dependency relationship between power and transportation networks. For fault tolerance and system optimization, Zhou Z et al. [9] studies the active fault-tolerant control strategy for distributed drive electric vehicles under multi-actuator failures, and Pryalukhin AF et al. [10] improves the operational reliability of dump truck units by considering the weakest components of the system. Rodríguez M et al. [11] enhances the fault impact analysis capability of substations through a systemic impact factor approach, optimizing fault management strategies by integrating theoretical analysis, experiments, and field tests. And Saleh Alyahyan et al. [12] conducts architectural and component impact analysis to establish a multi-level reliability evaluation framework, providing support for risk identification and architectural optimization of complex software systems; S. Zhang et al. [13] integrates SSVEP-BCI with augmented reality stimulus technology to develop a high-precision robot grasping system, breaking through the application limitations of traditional BCI systems; L. Yang et al. [14] integrates IoT and power electronics technology to construct a distributed collaborative control architecture, effectively improving the operational efficiency and reliability of power systems.

Neural network technology also plays a significant role in this aspect. One study proposes a bilinear neural network method for solving the analytical solution of the nonlinear strain wave equation, providing a neural network-based technical approach for the analytical solution of nonlinear wave-related problems [15]. Another study constructs a neural network-based symbolic computation method to realize the solution of the Korteweg–de Vries equation, expanding the application of neural networks in the field of symbolic solutions for nonlinear equations [16]. Additionally, a study adopts a bilinear residual network method to address the solution problem of nonlinear partial differential equations with variable coefficients, improving the efficiency and accuracy of solving

partial differential equations with complex coefficients [17]. The aforementioned studies provide neural network technical references for the solution optimization of the partial differential model for the failure rate of electrical components.

Meanwhile, the authors have also conducted some relevant previous studies. They constructed a quantum superposition model of event function states, which is applied to encryption and decryption operations, and analyzed the entanglement degree of the system fault evolution process, laying a theoretical foundation for the quantum description of fault evolution [18]. They proposed an intelligent calculation method based on the fault probability of edge devices to realize the evaluation of the fault probability of smart systems, providing a technical scheme for system-level fault probability calculation [19]. Under uncertain conditions, they analyzed the influences of factors and time on the System Fault Evolution Process (SFEP) by combining multimodal streaming data, offering a data-driven approach for the analysis of fault evolution under the action of multiple factors [20].

These studies, ranging from components to systems and from fault detection to fault-tolerant control, provide comprehensive references for the full-process management of faults in electrical systems.

However, the deficiency lies in the lack of calculation and analytical expressions for the failure rate of electrical components under multi-fault coupling, which makes it difficult to adapt to complex working conditions. There are problems such as the mutual induction of multiple fault mechanisms leading to non-linear coupling effects, resulting in difficulties in parameter fitting under multi-factor dynamic working conditions, the lack of real-time performance and poor adaptability of the failure rate model, and the lack of a unified parameter system. Ultimately, it is impossible to accurately determine the failure rate of electrical components under multi-fault coupling, and it is difficult to carry out model implementation.

To solve the above problems, the authors consider the constraints of electrical components in terms of physical materials, determine four fault modes and their influencing factors, and in the form on the basis of the fault rate analytical formula, the partial differential analytical formula of the fault rate is realized, so as to study the characteristics and influences of the change of the fault rate of electrical components under the condition of time variation.

2. Analytical description of the fault rate of electrical components

The faults of electrical components can be mainly divided into four types: electromigration, corrosion, hot carrier, and dielectric breakdown. Actual faults are also the superposition of these four faults to different degrees. The electromigration fault is that, under the condition of high current density, the metal material causes the atomic binding force to be broken due to the electron momentum transfer, leading to the failure of atomic transportation, such as voids and hillocks appearing in the lead. The fault is the cumulative damage of atomic transportation, and the action time needs to be considered, because it takes time for voids and hillocks to form and develop to cause failure and component fault. The corrosion fault is that the reaction between the metal and the environmental medium breaks through the chemical properties of the material. Humidity

and corrosive gas accelerate oxidation-reduction, causing the chemical corrosion of the metal to make the component fail. The action time of humidity and electrolyte needs to be considered. The formation of the electrolyte and the accumulation of corrosion products destroy the electrode, etc. with time, and then cause the electromigration fault of the component. The hot carrier fault is the effect of hot carrier action. The carrier energy superposition causes damage to the grid, damage to the lattice, and if the gate oxidation produces an interface state. The hot carrier fault is the effect of the damage level of energy, and the action time needs to be considered. The density of the interface state increases with time, and the threshold voltage shift exceeds the limit, resulting in component failure. The dielectric breakdown fault is that the electric field in the insulating material makes the electron avalanche effect reach the critical strength limit, and the exponential growth of the carrier density leads to the breakdown of the resistor. The fault is the critical breakdown of electrons, and the action time of the electric field needs to be considered. The acceleration of electrons, ionization, and the accumulation of carrier density to the threshold value take time, which will cause permanent breakdown and component failure.

Yu Z et al. [21], Thaduri A et al. [22] and Chenming Hu et al. [23] give the mean time to failure $MTTF$ of the failure process of electronic components. The MTTF of the electromigration fault $MTTF_{EM}$, the corrosion fault $MTTF_{COR}$, the hot carrier fault t, and the dielectric breakdown fault $MTTF_{TDDB}$ are as shown in Eq. (1).

$$\begin{cases} \text{MTTF}_{\text{EM}} = A \cdot J^{-2} \cdot exp\left(\dfrac{E_a}{kT}\right), \text{MTTF}_{\text{COR}} = A \cdot (R_H)^{-2} \cdot exp\left(\dfrac{E_a}{kT}\right), \text{MTTF}_{\text{HCI}} = B \cdot (I_{\text{sub}})^{-2} \cdot exp\left(\dfrac{E_a}{kT}\right) \\ \text{MTTF}_{\text{TDDB}} = \dfrac{\text{MTTF}_E + \text{MTTF}_{1/E}}{\text{MTTF}_E \cdot \text{MTTF}_{1/E}}, \text{MTTF}_E = t_0 \cdot exp\left(\dfrac{E_a}{kT} - \gamma E_x\right), \text{MTTF}_{1/E} = \tau_0 \cdot exp\left(\dfrac{G}{E_x}\right) \\ = \dfrac{\left(t_0 \cdot exp\left(\frac{E_a}{kT} - \gamma E_x\right) + \tau_0 \cdot exp\left(\frac{G}{E_x}\right)\right)}{\left(t_0 \cdot exp\left(\frac{E_a}{kT} - \gamma E_x\right) \times \tau_0 \cdot exp\left(\frac{G}{E_x}\right)\right)} \end{cases} \tag{1}$$

According to the fact that the failure rate λ and $\frac{\partial T}{\partial t} > 0$ are reciprocal to each other, the analytical equations of the electromigration fault λ_{EM}, the corrosion fault λ_{COR}, the hot carrier fault λ_{COR}, and the dielectric breakdown fault λ_{TDDB} are as shown in Eq. (2).

$$\begin{cases} \lambda_{EM} = \dfrac{1}{MTTF_{EM}} = \dfrac{1}{A \cdot J^{-2} \cdot exp(\frac{E_a}{kT})}, \lambda_{COR} = \dfrac{1}{MTTF_{COR}} = \dfrac{1}{A \cdot (R_H)^{-2} \cdot exp(\frac{E_a}{kT})} \\ \lambda_{HCI} = \dfrac{1}{MTTF_{HCI}} = \dfrac{1}{B \cdot (I_{sub})^{-2} \cdot exp(\frac{E_a}{kT})} \\ \lambda_{TDDB} = \dfrac{1}{MTTF_{TDDB}} = \dfrac{\left(t_0 \cdot exp\left(\frac{E_a}{kT} - \gamma E_x\right) \times \tau_0 \cdot exp\left(\frac{G}{E_x}\right)\right)}{\left(t_0 \cdot exp\left(\frac{E_a}{kT} - \gamma E_x\right) + \tau_0 \cdot exp\left(\frac{G}{E_x}\right)\right)} \end{cases} \tag{2}$$

In Eqs. (1) and (2), $\frac{\partial \lambda_p}{\partial t}$/μF·cm^{-2} is the coefficient related to the structure and material characteristics of the metal wire affected by electromigration. t/A·cm^{-2} is the current density. t/eV is the activation energy. $\frac{\partial T}{\partial t} > 0$/eV·K^{-1} is Boltzmann constant, approximately 8.617×10^{-5} eV·K^{-1}. $\int_0^t \lambda_p(t')dt'$/K is the absolute temperature. $\lambda_{\text{EM}} \propto J^2$/% is the relative humidity. B/cm·s^{-1} is the parameter of the sensitivity degree of

the reactive device to the hot carrier effect. I_{sub}/A is the substrate current. J/s is the time constant related to the dielectric material and the manufacturing process. τ_0/s is the initial time constant related to the dielectric material and the manufacturing process. $\frac{\partial \lambda_{HCI}}{\partial t} = \frac{2I_{sub}}{B} \cdot \frac{\partial I_{sub}}{\partial t} \cdot exp(\frac{E_a}{kT}) + \frac{\lambda_{HCI} \cdot E_a}{kT^2} \cdot \frac{\partial T}{\partial t}$/cm·mV^{-1} is the electric field acceleration factor. E_x/V·cm^{-1} is the electric field intensity applied on the insulating medium. G/MV·cm^{-1} is the parameter related to the defect of the medium and the electric field distribution.

Therefore, it can be seen that the formation of the above four typical faults of electrical components requires the cumulative action of time. At the same time, the four faults also involve many parameters in appearance. These parameters include constants and variables. Among them, the same variable may exist in the analytical formulas of multiple fault rates. When the changes of different variables are superimposed, the change of the component failure rate in the factor space [24, 25] presents a complex curved surface. Although it can reflect the change characteristics of the fault, the change is relatively complex. In particular, some variables are calibrated with time or according to time change. In conclusion, on the one hand, the fault of an electrical component is essentially due to the accumulation of various damages in time. On the other hand, the influence of the external environment can also be calibrated by time. Therefore, the operation time of the component in the fault analytical formula of the electrical component is of great importance research value.

3. Partial differential analytical expression of failure rate

According to the failure rate analytical formula and physical mechanism in the first section, combined with the multi-fault coupling effect, the partial differential analytical expression of the failure rate of electrical components is given.

For the failure rate of an electrical component, $\lambda_p = \lambda_{EM} + \lambda_{COR} + \lambda_{HCI} + \lambda_{TDDB}$. Its differential equation with respect to time t has the general form as shown in Eq. (3).

$$\frac{\partial \lambda_p}{\partial t} = \frac{\partial \lambda_{EM}}{\partial t} + \frac{\partial \lambda_{COR}}{\partial t} + \frac{\partial \lambda_{HCI}}{\partial t} + \frac{\partial \lambda_{TDDB}}{\partial t} + \frac{\partial \lambda_{inter}}{\partial t} \tag{3}$$

Among them, λ_p is the failure rate of the electrical component, /h; λ_{EM}, λ_{COR}, λ_{HCI}, λ_{TDDB} correspond to the failure rates of electromigration, corrosion, hot carrier, and dielectric breakdown faults, /h, respectively; $\frac{\partial \lambda_{inter}}{\partial t}$ is the multi-fault coupling term.

For the electromigration failure rate λ_{EM}, its partial derivative is shown in Eq. (4), which reflects the square effect of the current density J (the first term) and the exponential effect of the temperature T (the second term). The third term supplements the direct influence of the current change rate, which is consistent with the standard electromigration model.

$$\frac{\partial \lambda_{EM}}{\partial t} = \frac{2J}{A} \cdot \frac{\partial J}{\partial t} \cdot exp(\frac{E_a}{kT}) + \frac{\lambda_{EM} \cdot E_a}{kT^2} \cdot \frac{\partial T}{\partial t} + \frac{\lambda_{EM}}{J} \cdot \frac{\partial J}{\partial t} \tag{4}$$

For the corrosion failure rate λ_{COR}, its partial derivative is shown in Eq. (5),

$R_H > R_{Hth}$.

$$\frac{\partial \lambda_{COR}}{\partial t} = \frac{2R_H}{A} \cdot \frac{\partial R_H}{\partial t} \cdot exp(\frac{E_a}{kT}) + \frac{\lambda_{COR} \cdot E_a}{kT^2} \cdot \frac{\partial T}{\partial t} \tag{5}$$

When $R_H \leq R_{Hth}$, the partial derivative is 0. It reflects that after the humidity exceeds the threshold value R_{Hth}, it jointly accelerates the growth of the corrosion failure rate with the temperature.

For the hot carrier failure rate λ_{HCI}, its partial derivative is shown in Eq. (6), which reflects the failure rate caused by the hot carrier injection jointly affected by the substrate current I_{sub} and the temperature.

$$\frac{\partial \lambda_{HCI}}{\partial t} = \frac{2I_{sub}}{B} \cdot \frac{\partial I_{sub}}{\partial t} \cdot exp(\frac{E_a}{kT}) + \frac{\lambda_{HCI} \cdot E_a}{kT^2} \cdot \frac{\partial T}{\partial t} \tag{6}$$

For the dielectric breakdown failure rate λ_{TDDB}, its partial derivative is shown in Eq. (7), which reflects that the electric field intensity E_x affects the breakdown failure rate through the dual exponential action.

$$\frac{\partial \lambda_{TDDB}}{\partial t} = \gamma \cdot exp(\frac{G}{E_x} - \gamma E_x) \cdot (\frac{\partial E_x}{\partial t} \cdot \frac{G}{E_x^2} - \gamma \frac{\partial E_x}{\partial t}) + \frac{\lambda_{TDDB}}{t_0} \cdot \frac{\partial t_0}{\partial t} \tag{7}$$

For the multi-mechanism coupling term λ_{inter}, its partial derivative is shown in Eq. (8), where k_{int}, $k_{int'}$ are coupling coefficients, representing the synergistic effect of multi-fault mechanisms.

$$\frac{\partial \lambda_{inter}}{\partial t} = k_{int} \cdot \lambda_{EM} \cdot \lambda_{COR} \cdot \frac{\partial T}{\partial t} + k_{int'} \cdot \lambda_{HCI} \cdot \lambda_{TDDB} \cdot \frac{\partial E_x}{\partial t} \tag{8}$$

Substituting the partial derivative analytical formulas of the above failure rates into $\frac{\partial \lambda_{inter}}{\partial t}$, the complete partial differential analytical expression of the failure rate can be obtained. This represents the multi-fault coupling effect of the failure rate of electrical components under the participation of 4 fault types, and explains the characteristics of the failure rate through time variation. Finally, the partial differential analytical expression of the failure rate is constructed, as shown in Eq. (9).

$$\begin{aligned} \frac{\partial \lambda_p}{\partial t} &= \frac{2J}{A} \cdot \frac{\partial J}{\partial t} \cdot exp\left(\frac{E_a}{kT}\right) + \frac{\lambda_{EM} \cdot E_a}{kT^2} \cdot \frac{\partial T}{\partial t} + \frac{\lambda_{EM}}{J} \cdot \frac{\partial J}{\partial t} + \frac{2R_H}{A} \cdot \frac{\partial R_H}{\partial t} \cdot exp\left(\frac{E_a}{kT}\right) + \frac{\lambda_{COR} \cdot E_a}{kT^2} \cdot \frac{\partial T}{\partial t} \\ &+ \frac{2I_{sub}}{B} \cdot \frac{\partial I_{sub}}{\partial t} \cdot exp\left(\frac{E_a}{kT}\right) + \frac{\lambda_{HCI} \cdot E_a}{kT^2} \cdot \frac{\partial T}{\partial t} + \gamma \cdot exp\left(\frac{G}{E_x} - \gamma E_x\right) \cdot \left(\frac{\partial E_x}{\partial t} \cdot \frac{G}{E_x^2} - \gamma \frac{\partial E_x}{\partial t}\right) + \frac{\lambda_{TDDB}}{t_0} \cdot \frac{\partial t_0}{\partial t} \\ &+ k_{int} \cdot \lambda_{EM} \cdot \lambda_{COR} \cdot \frac{\partial T}{\partial t} + k_{int'} \cdot \lambda_{HCI} \cdot \lambda_{TDDB} \cdot \frac{\partial E_x}{\partial t} \end{aligned} \tag{9}$$

4. Time-dependence of failure rate

The above-mentioned partial differential analytical expression describes the dynamic evolution process of the failure rate with time. The partial derivative $\frac{\partial \lambda_p}{\partial t}$ represents the change rate of the failure rate λ_p with time, reflecting the attenuation rate of the reliability and the acceleration rate of the failure rate during the operation of the component. The failure rate λ_p (as in Eqs. (1) and (2)) was originally a static analytical expression (the failure rate when various factors are fixed). After introducing time t, it can depict the real-time response characteristics of the failure rate when environmental

parameters (such as temperature, electric field, and other factors) fluctuate with time, as shown in Eq. (3).

The physical meaning of the failure rate is the probability that a component fails within a unit time. Its mathematical definition is $\lambda(t) = \lim_{\Delta t \to 0} \frac{P(t<T\leq t+\Delta t)}{P(T>t)\Delta t}$, which implicitly contains the failure risk probability over time. Constructing the partial differential analytical formula with respect to t is the key to expanding the static model to a dynamic model. For example: when the temperature T increases with time, $\frac{\partial T}{\partial t} > 0$, and the temperature term ($\frac{\lambda \cdot E_a}{kT^2} \cdot \frac{\partial T}{\partial t}$) in the formula will make the failure rate increase with time in an accelerated manner, which conforms to the nature of the temperature index affecting the failure rate. Another example is in the analysis of the transient working conditions of components, such as the sudden change of temperature in the startup/shutdown of components and the sudden increase of electric field intensity during lightning strikes. Through the analytical formula, the transient change of the failure rate can be calculated, the failure risk can be evaluated, and the integral $\int_0^t \lambda_p(t^{'})dt^{'}$ can approximately characterize the cumulative failure probability of the component within time t, providing dynamic model support for the life assessment of components.

Time t is a key variable connecting the static failure rate model with the actual working conditions. Its introduction enables the analytical formula to describe the evolution of multiple physical factors (various faults) with time-varying coupling terms, providing a theoretical method for engineering practice to monitor and control the failure rate from the time dimension.

5. Multi-fault coupling terms construction

In the process of electrical component failure, the multi-fault coupling effect refers to the phenomenon that multiple fault modes interact and synergistically accelerate fault evolution. Of course, the interior of multi-fault coupling operates according to physical constraints and mechanisms, and the exterior is triggered by the combined action of multiple factors. Combined with the fault types of electrical components, the multi-fault coupling terms are explained.

The aforementioned electrical component fault assumes that four types (electromigration, corrosion, hot carrier, dielectric breakdown) of faults are independently superimposed, $\lambda_p = \lambda_{EM} + \lambda_{COR} + \lambda_{HCI} + \lambda_{TDDB}$. However, under actual working conditions, different faults can promote each other through some ways (such as common mechanisms and factors). For example, high temperature (T) enhances the activity of metal ions, and high humidity (R_H) provides an electrolyte environment, and the two jointly accelerate the rate of electrochemical corrosion. After electromigration causes damage to the wire surface, the dielectric is more likely to be invaded, forming an ”electromigration-corrosion” coupling failure. A strong electric field (E_x) accelerates the production of hot carriers on the lead; at the same time, hot carriers inject into the dielectric, which will reduce the breakdown threshold of dielectric breakdown, forming a hot carrier-dielectric breakdown coupling failure.

The typical fault coupling terms introduced in the failure rate analytical formula of electrical components are as follows. The electromigration-corrosion coupling term $\frac{\partial \lambda_{EM-COR}}{\partial t} = k_{int} \cdot \lambda_{EM} \cdot \lambda_{COR} \cdot \frac{\partial T}{\partial t}$, where k_{int} is the electromigration-corrosion

coupling coefficient (/K⁻¹), reflecting the amplifying effect of high temperature on the electromigration-corrosion synergy; $\lambda_{EM} \cdot \lambda_{COR}$ represents the mutual promotion when the two faults occur simultaneously, and $\frac{\partial T}{\partial t}$ is the temperature change rate. When the temperature rises ($\frac{\partial T}{\partial t} > 0$), the wire damage caused by electromigration and the material deterioration caused by corrosion mutually enhance each other. The hot carrier-breakdown coupling term $\frac{\partial \lambda_{HCI-TDDB}}{\partial t} = k_{int'} \cdot \lambda_{HCI} \cdot \lambda_{TDDB} \cdot \frac{\partial E_x}{\partial t}$, where $k_{int'}$ is the hot carrier-breakdown coupling coefficient (/(V/cm)⁻¹), describing the accelerating effect of the strong electric field on the hot carrier-breakdown synergy; $\lambda_{HCI} \cdot \lambda_{TDDB}$ represents the mutual promotion of hot carrier damage and dielectric breakdown, and $\frac{\partial E_x}{\partial t}$ is the electric field change rate. When the electric field is enhanced ($\frac{\partial E_x}{\partial t} > 0$), the increase in the interface state density caused by hot carrier injection and the electron avalanche effect of dielectric breakdown interact with each other, and the failure rate increases exponentially.

According to estimation, after considering the coupling terms, the actual failure probability may be 30%–50% higher than the independent calculation value (such as in high-temperature and high-humidity working conditions). In engineering, in harsh environments such as aerospace, multi-fault coupling cannot be ignored. The failure rate needs to be corrected through coupling terms to avoid insufficient design margin; at the same time, suppressing temperature and humidity (not simply controlling individually) can more effectively reduce the coupling failure risk. The multi-fault coupling terms are a supplement to the independent fault model and need to be selectively introduced according to the engineering site to improve the accuracy of failure rate prediction and provide more accurate theoretical support for the design of highly reliable electrical components.

6. Coupling coefficient determination

Furthermore, the coupling coefficients k_{int} and $k_{\text{int}'}$ are used to quantify the intensity of the synergistic effect between multi-fault mechanisms, and need to be constructed and solved in combination with experimental data and theoretical guidance. The following gives the calculation methods of two typical coupling coefficients from the perspectives of physical mechanisms and engineering practice.

For the electromigration-corrosion coupling coefficient k_{int}, it is the coupling of the action of electromigration (λ_{EM}) and corrosion (λ_{COR}), and its essence is the electrochemical acceleration effect driven by temperature. According to the Arrhenius model [26], the influence of temperature on the corrosion rate can be expressed as $\lambda_{\text{COR}}(T) = \lambda_{\text{COR},0} exp\left(\frac{E_a}{RT}\right)$, among them: $\lambda_{COR,0}$ is the corrosion failure rate under (reference conditions), E_a is the activation energy of the corrosion reaction, and R is the gas constant. When electromigration causes damage to the metal surface (such as micro-cracks), the contact area of the corrosion medium increases, and the coupling effect can be quantified through the cumulative damage area. Assuming that the electromigration damage area is proportional to the square of the current density ($S_{EM} \propto J^2$), then the coupling coefficient: $k_{\text{int}} = \frac{1}{A} \cdot \frac{Q_{\text{COR}}}{RT^2} \cdot \frac{J^2}{J_0^2}$, J_0 is the reference current density (such as the rated working current density); $Q_{COR} \approx 0.8$eV (activation energy of typical metal electrochemical corrosion).

For the hot carrier-breakdown coupling coefficient $k_{\text{int}'}$, it is the coupling of hot carriers (λ_{HCI}) and dielectric breakdown (λ_{TDDB}), originating from the accumulation of dielectric defects caused by hot carrier injection. The electric field threshold $E_{BD,\,th}$ for dielectric breakdown decreases with the increase of defect density, satisfying $E_{\text{BD,th}} \propto 1/\sqrt{N_{\text{defect}}}$. Combining with the dielectric breakdown model, the coupling coefficient is $k_{\text{int}'} = \gamma \cdot \frac{G}{E_x^2} \cdot \frac{\alpha \cdot I_{\text{sub}}}{B} \cdot exp\left(-\frac{E_{\text{defect}} - E_a}{kT}\right)$, where: $E_{\text{defect}} \approx 1.2$ eV (formation energy of typical dielectric defects).

Considering the difficulty in calculating the above coupling coefficients, the following analysis is made. For consumer-level electronic components, when the temperature $T < 400K$ and the current density $J < 500$ A/cm^2, the coupling coefficient can be approximately $k_{\text{int}} \approx 5 \times 10^{-4} \cdot \frac{J^2}{T^2}$. For the failure analysis of the gate oxide layer of integrated circuits, when the electric field intensity $E_x < 10^7$ V/cm and the substrate current $I_{sub} < 1$ mA, the coupling coefficient can be approximately $k_{\text{int}'} \approx 2 \times 10^{-6} \cdot \frac{I_{\text{sub}} \cdot G}{E_x^2 \cdot T}$. These approximations only consider the single dominant factor of temperature/electric field, without including the cross-coupling of multiple parameters (such as the synergistic effect of temperature and electric field); they are suitable for working conditions with slowly changing parameters and do not cover extreme scenarios such as transient impacts (like lightning strikes, short circuits).

7. Case analysis

The parameters of a certain electrical component, including its own parameters and environmental parameters, are summarized as follows: Constant A = 2μF·cm^{-2}; Current density J = 150 A·cm^{-2}; Activation energy $E_a = 0.7$ eV; Boltzmann constant $k = 8.617 \times 10^{-5}$ eV$\cdot K^{-1}$; Absolute temperature $T = 290K$; Relative humidity $R_H = 30\%$; Hot carrier effect constant $B = 10$ cm $\cdot$ s^{-1}; Substrate current $I_{sub} = 2 \times 10^{-5}$ A; Electric field acceleration factor $\gamma = 700$ cm $\cdot$ mV^{-1}; Electric field intensity in the gate oxide layer $E_x = 9 \times 10^5$ V $\cdot$ cm^{-1}; Initial time constant $\tau_0 = 1.0 \times 10^{-11}$ s; Model constant $G = 3.5$ MV $\cdot$ cm^{-1}; Time constant $t_0 = 6.3 \times 10^{14}$ s. The time variation range is 0–300 s. The temperature change rate is $0.05K \cdot$ s^{-1}; the current density change rate is 1.5 A $\cdot$ cm^{-2} $\cdot$ s^{-1}; the humidity change rate is $0.003\% \cdot$ s^{-1}; the substrate current change rate is 2×10^{-8} A $\cdot$ s^{-1}; the electric field change rate is 20 V $\cdot$ cm^{-1} $\cdot$ s^{-1}.

According to formulas (1) and (2), substituting the above parameters, the failure rates of the four types of faults are obtained. At the initial moment $t = 0$, the electromigration failure rate is 2.766959×10^{-5}/h; the corrosion failure rate is 1.106784×10^{-14}/h; the hot carrier failure rate is $9.838076e \times 10^{-20}$/h; the dielectric breakdown failure rate is 0. Therefore, the failure rate of the electrical component at this time is approximately 2.766959×10^{-5}/h. According to the analytical formulas of the coefficients of two typical coupling terms, substituting the parameters, the electromigration-corrosion $k_{int} = 1.337693 \times 10^{-4}$; the hot carrier-breakdown $k_{\text{int}'} = 5.959988 \times 10^{-25}$; According to Eq. (3), the partial derivative of the failure rate of the electrical component $\frac{\partial \lambda_p}{\partial t} = 1.185598 \times 10^{18}$/h·s^{-1}.

When the observation time variation range is 0–300 s, the relevant results are plotted as curves according to this time period. The following are respectively the time-variation curve of the failure rate of the electrical component, the time-variation

curves of the two coupling coefficients, and the time-variation curve of the derivative of the component failure rate with respect to time, as shown in the following figures.

Figure 1 shows the component failure rate curve, which rises approximately exponentially with time (increasing from 10^{-5} to 2×10^{-3}/h within 0–300 s), reflecting the cumulative effect of parameters. Temperature, current density, etc. increase with time, and the failure rate is amplified through the exponential term and the square of the current. After 100 s, the slope of the curve increases significantly, corresponding to the growth of the partial derivatives caused by dT/dt and dJ/dt. This indicates that the parameters enter a nonlinear acceleration stage, and the reliability of the component decreases rapidly.

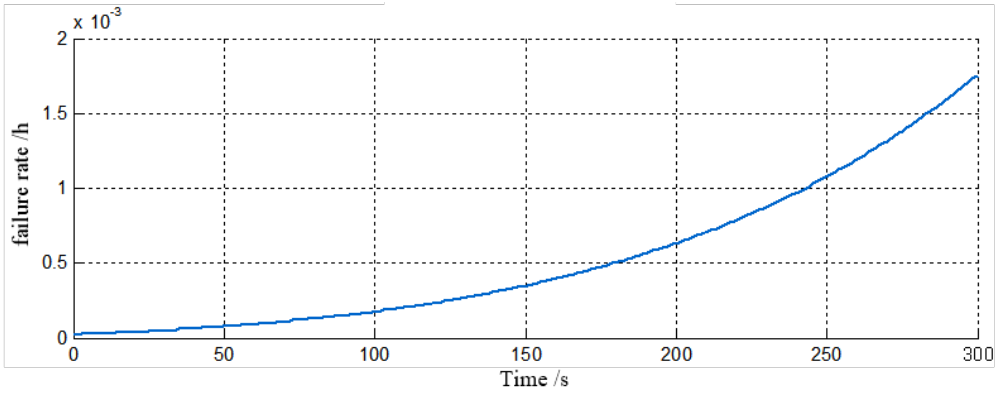

Figure 1. Time-varying curve of failure rate of electrical components.

Figure 2 shows the coupling coefficient curves. For the electromigration-corrosion coupling coefficient, it shows a rapid upward trend (increasing from 0 to 2×10^{-3} within 300 s). Because the coupling coefficient $k_{\text{int}} \propto J^2/T^2$, the linear growth of the current density J and the quadratic growth of the temperature T together lead to its exponential amplification. This shows that the synergistic effect of electromigration and corrosion faults increases with time, and the two types of faults change from independent development to mutual acceleration. It is necessary to focus on monitoring the current and humidity parameters. For the hot carrier-breakdown coupling coefficient, it shows a linear growth (increasing from 5.8×10^{-11} to 7.2×10^{-11} within 300 s). Because $k_{\text{int}'} \propto I_{\text{sub}}/(E_x^2 T)$, the linear growth of the substrate current I_{sub} and the quadratic growth of the electric field E_x offset part of the temperature effect, so the growth is flat. This shows that the coupling effect of hot carriers and dielectric breakdown is weak and stable, has less impact on the component failure rate, and can be used as a secondary monitoring item.

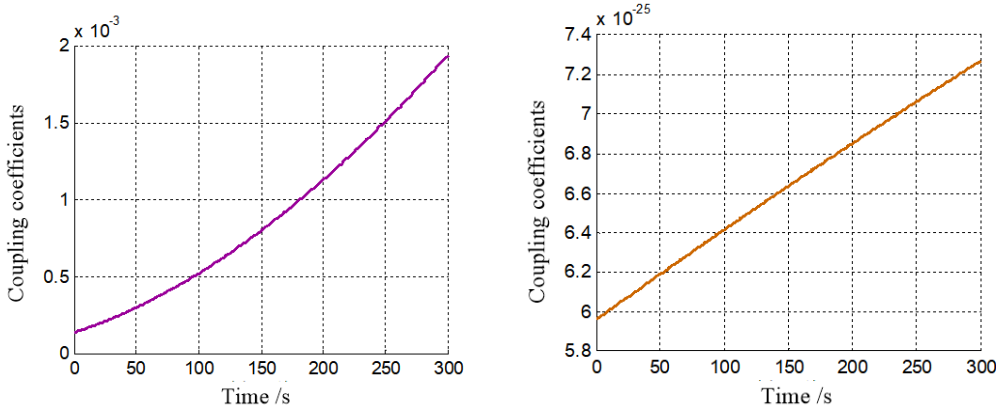

(a) k_{int} **(b)** $k_{\text{int}'}$

Figure 2. Variation curves of two coupling coefficients with time.

Figure 3 shows the failure rate derivative curve, which is a parabolic trend that first increases and then decreases. The derivative reaches a peak around 100 s, corresponding to the collaboration-offset process of the parameter change rate and the exponential term. In the first 100 s, the increase in temperature T and current density J makes the exponential term of the derivative dominant, and the partial derivative rises; after 100 s, the increase in the electric field E_x makes thegrowth leads to a decrease in the derivative of the dielectric breakdown failure rate, offsetting the growth of electromigration/corrosion and causing the derivative to decline. This indicates that the peak point is the critical life point. Around 100 s is the transition from the early fault stage to the accelerated failure stage of the component. Although the derivative decreases, it does not mean that the failure rate reduces; the total failure rate is still increasing, but the growth rate slows down. However, the irrecoverable degradation of component reliability still occurs.

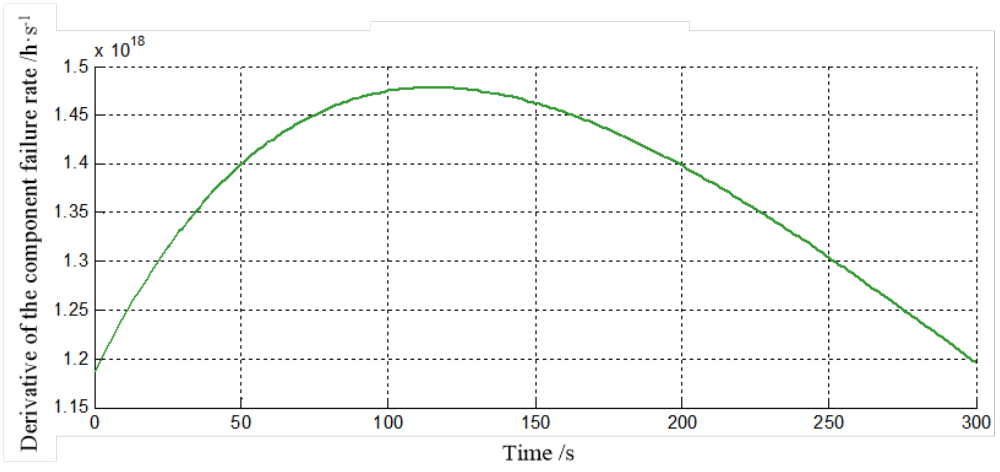

Figure 3. Variation curve of the derivative of the component failure rate over time.

The research achievement has the advantages of integrating multiple physical mechanisms, describing dynamic time-dependence, and combining physical mechanisms with engineering practice. It can consider the coupling effects of multiple physical mechanisms such as electromigration, and the mutual promotion of cross-field coupling, making the traditional model closer to the actual working conditions. It can also introduce

time-varying fault models as dynamic incentive to solve the parameter micro-analysis of fault rate changes, providing a theoretical basis for component fault analysis. The constructed micro-decomposition analytical formula combines physical theory with engineering practice. However, it also has disadvantages such as model simplification assumptions, complex parameter determination, and high computational complexity, and does not cover all cross-couplings. Parameter dependence on experimental calibration exists, and the universality of the model still needs to be improved. The research significance lies in constructing a dynamic analysis framework, which can be used to guide research and engineering applications such as life prediction and design optimization of electrical components.

8. Discussion

The innovations and improvements of this work can be summarized as follows.

1) For the first time, the coupling effects of four types of faults (e.g., electromigration, corrosion) are integrated into the partial differential model of failure rate, and an analytical expression with coupling terms (Eq. (3)) is derived, breaking the limitation of single-fault analysis.
2) The engineering approximation formula for coupling coefficients (Eq. (6)) is proposed, which simplifies calculations under conventional working conditions while retaining the dynamic coupling characteristics of multiple faults, balancing accuracy and engineering practicability.
3) An analytical framework for the time derivative of failure rate is established to quantify the impact of parameter time change rate on failure rate, enabling dynamic failure trend prediction and making up for the deficiency of static models.

Further discussions on several necessary issues are presented herein to supplement the theoretical and practical implications of the proposed model. The limitations of the proposed method in terms of microstructural randomness, localized defects, and the discreteness of damage nucleation are explained as follows, and feasible improvement schemes are provided.

The partial differential analytical model for the failure rate of electrical components under multi-fault coupling proposed in this study adopts continuum and mean-field assumptions, whose rationality stems from the adaptation of research objectives to engineering needs. The core of this study is to construct an analytical framework for the synergistic effect of multi-fault coupling and time-dependent dynamic effects, filling the gap in existing research where there is a lack of quantifiable analytical expressions for the failure rate under multi-factor coupling. The continuum assumption treats material properties as macroscopic average quantities, avoiding excessive introduction of microparameters that would lead to a surge in model complexity and loss of analytical capability. The mean-field assumption condenses the interaction of multiple faults into quantifiable coupling terms, and finally derives the partial differential analytical expression shown in Eq. (3). This provides theoretical support for real-time failure rate assessment in engineering scenarios, conforms to the scientific development logic of models that first solve macroscopic coupling quantification and then gradually optimize

accuracy, and can meet the basic needs of the industry for component reliability design.

To address the limitations of the model, such as neglecting microstructural randomness, localized defects, and the discreteness of damage nucleation, future improvements can be made from three aspects: First, introduce microparameter correction factors. For example, add a defect density correction term and a local electric field distortion factor to the failure rate formulas of electromigration and dielectric breakdown, respectively, to realize the coupling between macroscopic failure rate and microdefect states while retaining the analytical characteristics of the model. Second, integrate probabilistic statistical methods. Simulate key microscale random parameters through Monte Carlo sampling, expand the deterministic model into a probabilistic analytical model, quantify the lifetime scatter, and output failure rate prediction results with confidence intervals. Third, construct a macro-micro multiscale experimental system. Combine component lifetime tests with in-situ microscale observations to calibrate model parameters and capture early anomaly-driven failure signals, thereby further improving the model's accuracy and engineering applicability.

9. Conclusion

1) The research clarifies that the faults of electrical components are mainly composed of four types: electromigration, corrosion, hot carrier, and dielectric breakdown. It gives their mean time to failure and failure rate analytical formulas, revealing that the essence of faults is the time accumulation of various damages. Based on this, a partial differential analytical formula of the failure rate is constructed. Considering the coupling effects of multiple factors, the partial differential analytical formulas for electromigration, corrosion, hot carrier, and dielectric breakdown faults are derived. By introducing multi-fault coupling terms, the dynamic influences of parameters such as temperature and current density on the failure rate are reflected, providing a theoretical basis for component fault analysis.
2) The research on the partial differential analytical formula of the failure rate can study dynamic faults, reflect the reliability attenuation rate of components, and expand the static model to a dynamic model. It is found that the multi-fault coupling effect is significant during the failure process of components. For example, electromigration-corrosion and hot carrier-breakdown synergistically accelerate fault occurrence. Considering the coupling terms, the actual failure rate is 30%–50% higher than the independent calculation. The coupling coefficient can quantify the intensity of the synergistic effect, and through physical mechanism and engineering practice, the analytical formulas and approximate forms of the electromigration-corrosion coupling coefficient and the hot carrier-breakdown coupling coefficient are given.
3) For a certain electrical component calculation, the initial electromigration failure rate is 2.766959×10^{-5}/h, the electromigration-corrosion coupling coefficient is 1.337693×10^{-4}, the hot carrier-breakdown coupling coefficient is 5.959983×10^{-25}, and the failure rate derivative is 1.185598×10^{18}/h·s^{-1}. The curves show that the failure rate approximately increases exponentially; after 100 s, the slope of the

curve increases, and the reliability decreases rapidly; the electromigration-corrosion coupling coefficient is amplified exponentially, and the hot carrier-breakdown coupling coefficient grows linearly; the failure rate derivative first increases and then decreases, reaching a peak at 100 s, which is the critical life point. After that, the growth rate slows down, but the reliability continues to deteriorate. Finally, the advantages, disadvantages, and significance of the research are summarized.

Author contributions: Conceptualization, methodology, formal analysis, writing—review and editing, supervision, TC; software, validation, investigation, writing—original draft preparation, project administration, funding acquisition, SL; resources, data curation, visualization, PW. All authors have read and agreed to the published version of the manuscript.

Funding: Liaoning Provincial Science and Technology Plan Joint Program (Natural Science Foundation-General Program 2025-MSLH-584); Special Foundation for Basic Scientific Research Business of Liaoning Provincial Undergraduate High-level Universities (LJ212410144051; LJ212410144032).

Acknowledgment: The authors wish to thank all his friends for their valuable critics, comments and assistance with this paper.

Conflict of interest: The authors declare no conflict of interest.

References

1. Dwivedi D, Victor Sam Moses Babu K, Kronman D, et al. Fault detection and prediction in electrical distribution system using nonlinear dynamics and machine learning models. Energy Science. 2025; 2550005. doi: 10.1142/S297237952550005X
2. Ilyushin P, Gaisin B, Shahmaev I, et al. An algorithm for identifying the possibilities of cascading failure processes and their development trajectories in electric power systems. Algorithms. 2025; 18(4): 183. doi: 10.3390/a18040183
3. Lou Y-L, Zhang K, Feng X-H, et al. Research on damaged unit detection of lithium battery thermal management system. International Journal of Heat and Fluid Flow. 2025; 115: 109857. doi: 10.1016/j.ijheatfluidflow.2025.109857
4. Shuhui W, Zhenpo W, Zhaosheng Z, et al. Fault cause inferences of onboard lithium-ion battery thermal runaway using convolutional neural network. Energy. 2025; 320: 135328. doi: 10.1016/j.energy.2025.135328
5. Qi M, Jin L, Yao H, et al. Recent progress on electrical failure and stability of perovskite solar cells under reverse bias. Acta Physico-Chimica Sinica. 2025; 41(8): 100088. doi: 10.1016/j.actphy.2025.100088
6. Ren L, Zhang X, Lan X. Research on the mechanism and dynamic characteristics of intermittent failure of electrical connectors. Applied Sciences. 2025; 15(6): 3328. doi: 10.3390/app15063328
7. An H, Xu G, Sun Z, et al. Multi-perspective failure mode and effects analysis based on rough number projection. Engineering Failure Analysis. 2025; 169: 109192. doi: 10.1016/j.engfailanal.2024.109192
8. Lu Q-C, Wang S, Xu P-C, et al. Modeling the dependency relationship of coupled power and transportation networks. Energy. 2025; 320: 135330. doi: 10.1016/j.energy.2025.135330
9. Zhou Z, Chen M, Zhang G, et al. Research on active fault tolerant control strategy for distributed drive electric vehicles based on multi-actuator failure. Engineering Letters. 2025; 33(2): 320–329. Available online: https://www.engineeringletters.com/issues_v33/issue_2/EL_33_2_11.pdf
10. Pryalukhin AF, Martyushev NV, Malozyomov BV, et al. Improvement of operational reliability of units and elements of dump trucks taking into account the least reliable elements of the system. World Electric Vehicle Journal. 2024; 15(8): 365. doi: 10.3390/wevj15080365
11. Rodríguez M, Crespo A, González-Prida V. Enhancing prescriptive capabilities in electrical substations: a systemic impact factor approach for failure impact analysis. Energies. 2024; 17(4): 770. doi: 10.3390/en17040770

12. Alyahyan S, Alatawi MN, Alnfiai MM, et al. Software reliability assessment: an architectural and component impact analysis. Tsinghua Science and Technology. 2025; 30(2): 908–925. doi: 10.26599/TST.2024.9010101
13. Zhang S, Chen Y, Zhang L, et al. Study on robot grasping system of SSVEP-BCI based on augmented reality stimulus. Tsinghua Science and Technology. 2023; 28(2): 322–329. doi: 10.26599/TST.2021.9010085
14. Yang L, Ma B, Yuan L, et al. Effective application of IoT power electronics technology and power system optimization control. Tsinghua Science and Technology. 2024; 29(6): 1763–1775. doi: 10.26599/TST.2023.9010124
15. Muslim H, Ahmed N, Macías S, et al. On the analytical solution of the nonlinear strain wave equation through the bilinear neural network method. Evolutionary Intelligence. 2025; 18(5): 97. doi: 10.1007/s12065-025-01068-0
16. Xie X-R, Zhang R-F. Neural network-based symbolic calculation approach for solving the Korteweg–de Vries equation. Chaos, Solitons & Fractals. 2025; 194: 116232. doi: 10.1016/j.chaos.2025.116232
17. Wu X-S, Liu J-G. Solving the variable coefficient nonlinear partial differential equations based on the bilinear residual network method. Nonlinear Dynamics. 2024; 112(10): 8329–8340. doi: 10.1007/s11071-024-09472-4
18. Li S, Cui T. Quantum superposition of event function states for encryption-decryption and the entanglement degree of system fault evolution process. Tsinghua Science and Technology. 2025; doi: 10.26599/TST.2024.9010113
19. Li S, Cui T, Viriyasitavat W. Edge device fault probability based intelligent calculations for fault probability of smart systems. Tsinghua Science and Technology. 2024; 29(4): 1023–1036. doi: 10.26599/TST.2023.9010085
20. Li S, Cui T. Effect analysis of factors and time on SFEP using multimodal streaming data under uncertain conditions. Tsinghua Science and Technology. 2025; doi: 10.26599/TST.2024.9010156
21. Yu Z, Zhonghua C, Guangyao L, et al. Failure mode analysis of electronic equipment based on PoF model and FTA. Modern Defence Technology. 2023; 51 (04): 86–96.
22. Thaduri A, Verma AK, Gopika V, et al. Reliability prediction of semiconductor devices using modified physics of failure approach. International Journal of System Assurance Engineering and Management. 2013; 4(1): 33–47. doi: 10.1007/s13198-013-0146-9
23. Chenming Hu, Simon C. Tam, Fu-Chieh Hsu, et al. Hot-electron-induced MOSFET degradation-Model, monitor, and improvement. IEEE Transactions on Electron Devices. 1985; 32(2): 375–385. doi: 10.1109/T-ED.1985.21952
24. Fanhui Z, Guangshan H, Hui S, et al. A causal probabilistic inference classification algorithm based on factor space theory. CAAI Transactions on Intelligent Systems. 2024; 19 (04): 1042–1051. Available online: https://tis.hrbeu.edu.cn/en/oa/darticle.aspx?type=view&id=202206004
25. Jinhui L, Sizong G, Peizhuang W. Construction of the intuitionistic fuzzy concept extension based on factor space and its application in decision making. Operations Research and Management Science. 2023; 32 (05): 175–180. Available online: http://www.jorms.net/CN/10.12005/orms.2023.0166 (in Chinese)
26. Yang Y, Weijun W, Liu Y, et al. Hot compression deformation behavior of extruded Mg-Mn-Ce alloy based on Arrhenius and BP-ANN models. Rare Metal Materials and Engineering. 2025; 54 (02): 517–523. Available online: http://www.rmme.ac.cn/rmme/article/abstract/20240547 (in Chinese)